Oxidation of Fe-2.25Cr-1Mo in presence of KCl(s) at 400 °C – Crack formation and its influence on oxidation kinetics

Corrosion Science 163 (2020) 108234

Contents lists available at ScienceDirect

Corrosion Science

journal homepage: www.elsevier.com/locate/corsci

Oxidation of Fe-2.25Cr-1Mo in presence of KCl(s) at 400 °C – Crack formation and its influence on oxidation kinetics

A. Persdotter*, M. Sattari, E. Larsson, M.A. Olivas Ogaz, J. Liske, T. Jonsson

Energy and Materials, Department of Chemistry and Chemical Engineering, Chalmers University of Technology, S-412 96 Gothenburg, Sweden

ARTICLE INFO

Keywords:
High temperature corrosion
Low alloy steel
Oxidation
Chlorination
Alkaline corrosion
STEM

ABSTRACT

Accelerated corrosion of boiler equipment remains a challenge for efficiently utilising biomass- and waste for power production. To overcome this challenge a better understanding of the influence of corrosive species present is required. This study focuses on the influence of KCl(s) on corrosion of Fe-2.25Cr-1Mo at 400 °C. This is done by well-controlled laboratory exposures and detailed microstructural investigation with ion and electron microscopy (TEM, FIB, SEM, EDX, XRD, TKD). The scale microstructures are linked to oxidation kinetics. The results indicate that KCl(s) increases the ionic diffusion through the oxide scale as well as introduces cracks and delamination resulting in a rapid periodic growth process.

1. Introduction

Utilising renewable and CO_2 neutral fuels such as biomass- and waste for power production is an attractive alternative to power plants burning fossil fuels. The combustion of biomass and waste, however, results in the release of corrosive species such as HCl and alkali chlorides [1,2]. This puts high demands on the corrosion resistance of the alloys used for boiler equipment such as waterwalls and superheaters.

In order to limit the corrosion and increase the lifetime of boilers the power plants using renewable fuels are often operated at a considerably lower steam temperature than those using fossil fuels. This results in decreased electrical efficiency, which makes biomass and waste less competitive towards fossil fuels. Another way to limit corrosion of boiler equipment is to use more corrosion resistant materials, such as stainless steels. However, this is costly and in order to make biomass- and waste an economically favourable alternative to fossil fuels the use of less expensive materials, such as low alloyed steels (e.g. Fe-2.25Cr-1Mo), as well as higher operating temperatures are interesting goals. To make this possible while maintaining a reasonable lifetime of the boiler equipment it is necessary to increase the understanding of the underlying mechanisms of the rapid corrosion of low alloyed steels.

The influence of alkali chlorides and other chlorine containing compounds on high temperature corrosion has previously been studied extensively on both pure iron [3–7], stainless [2–5,7–20] and low alloyed steels [2,4,5,8,10,11,13,21–27]. While it is well-known that chlorine containing compounds cause corrosion of all these materials, the underlying mechanisms of both chlorine and alkali species are still under debate. The corrosion resistance of stainless steels relies on the ability to form a protective Cr-rich oxide scale ($(Cr_xFe_{1-x})_2O_3$). Previous studies on stainless steels [12,15,16,18,19] have shown that alkali, specifically potassium, influences high temperature corrosion by depleting the protective Cr-rich scale to form potassium chromates (see reaction (1)). This results in breakdown of the protective Cr-rich oxide and the formation of a less protective iron rich scale.

$$4xKCl(s) + (Cr_x, Fe_{1-x})_2O_3(s) + \frac{3x}{2}O_2(g) + 2xH_2O(g) \rightarrow \longrightarrow 2xK_2CrO_4(s) + (1-x)Fe_2O_3(s) + 4xHCl(g) \quad (1)$$

For low alloyed steels the amount of chromium in the alloy is not sufficient to form this protective Cr-rich oxide. Instead the scale formed is iron rich consisting of a Fe_2O_3 layer on top of an $(Fe, M)_3O_4$ (< 570 °C). Thus, the depletion of chromium of the oxide does not explain the observed accelerated corrosion of low alloyed steels in presence of alkali chlorides. For low alloyed steels the chlorine is instead considered the most corrosive species and the influence of alkali remains unknown.

The so called active oxidation, i.e. the chlorine cycle, initially proposed by McNallan et al. [28] and further developed by Grabke et al. [8], is one mechanism proposed to explain the oxide morphology and microstructure in the presence of chlorine in a wide temperature and material range [2–4,6,8–11,21,28]. Active oxidation is a cyclic process where chlorine is proposed to be released at the sample surface as Cl_2 molecules (by reaction with O_2) and then penetrate the oxide scale to form volatile transition metal chlorides at the scale/metal interface

* Corresponding author.
E-mail address: amaper@chalmers.se (A. Persdotter).

https://doi.org/10.1016/j.corsci.2019.108234
Received 5 February 2019; Received in revised form 16 September 2019; Accepted 20 September 2019
Available online 24 September 2019

(low pO_2). Because of the high vapour pressure of the metal chlorides they will then diffuse outwards through the scale and decompose into a porous metal oxide and Cl_2 (see reaction (2)) closer to the scale surface (high pO_2). The released Cl_2 is proposed to partly diffuse back to the scale/metal interface and continue the oxidation process without self-consumption acting like a corrosion catalyst.

$$2MCl_2(g) + \frac{3}{2}O_2(g) \rightarrow M_2O_3(s) + 2Cl_2(g) \quad (2)$$

Folkeson et al. [14,24] proposed an alternative to the chlorine cycle, here referred to as the electrochemical mechanism. For low alloyed steels [24] this mechanism proposes KCl to react with O_2 and H_2O on the scale surface to form potassium hydroxide and release chlorine ions (Cl^-). The Cl^- is suggested to diffuse through grain boundaries towards the metal to form metal chlorides throughout the scale (at the grain boundaries and at the scale/metal interface). The accelerated corrosion observed in presence of KCl is proposed to be caused by that $FeCl_2$ at the grain boundaries facilitates transport of both iron and oxygen ions.

Chlorine containing compounds may also form mixtures with low melting points causing rapid spread of corrosive species over the surface and accelerated corrosion due to the liquid phase [4,6,25,29]. Jonsson et al. [25] studied the corrosion mechanisms of a low alloyed steel (Fe-2.25Cr-1Mo) close to the deposited KCl crystals by in-situ ESEM showing that the KCl(s) started to react well below 400 °C and proposed that the corrosive species spread over the sample surface by formation of a eutectic mixture ($KCl/FeCl_2$). The study suggested the local corrosion reaction (in the vicinity of the KCl particles) to be initiated by the reaction of KCl with O_2 forming KOH (or K_2O) and $KFeO_2$ as well as Cl^- ions. The general corrosion, i.e. growth of the base oxide (away from the KCl particles), was proposed to be caused by an increased diffusion rate through the oxide due to the presence of Cl^- ions at the oxide grain boundaries, in similarity to Folkeson et al. [24]. However, there was no evidence for formation of iron chlorides or Cl^- at the grain boundaries. A recent study by Cantatore et al. [30] showed that chlorine could also permeate the magnetite oxide through lattice diffusion, which could open up for new mechanistic insights on the influence of chlorine on the oxide scale growth.

Several previous corrosion studies performed on the low alloyed steel Fe-2.25Cr-1Mo in presence of KCl(s) [10,24,26,31] showed accelerated corrosion and indications of crack formation and/or delamination. However, the microstructure and the chemical composition of the oxide scale was not studied in detail and the mechanisms for the observed accelerated corrosion and influence on the total growth process is still under investigation. The oxide scales formed on low alloyed steels and pure iron under oxidising conditions at 600 °C have been shown to be multi-layered and composed of a thin outward growing Fe_2O_3 (corundum), a thicker outward growing Fe_3O_4 and an inward growing spinel oxide [25,32–35]. The inward growing spinel formed on iron was pure Fe_3O_4 while chromium was present in the inward growing spinel ($(Fe,Cr)_3O_4$) on chromium containing low alloyed steels. Chromium, was suggested to remain at its original position due to the relatively slow diffusivity of Cr^{3+} ions in the spinel phase, as compared to iron [36,37]. The influence of a cracked or partly delaminated oxide scale would change the conditions for diffusing species through the scale, affecting the corrosion rate extensively. In order to better understand the reason for the accelerated growth rate observed on low alloyed steels in the presence of alkali chlorides it is of great importance to further investigate the microstructural changes in the oxide scale.

In this study a detailed microstructural investigation in combination with an in-situ oxide growth study aims to link the delamination and scale microstructure to the oxidation kinetics and the observed accelerated corrosion. Explaining the influence of crack formation and scale delamination would contribute with essential information for e.g. the development of reliable kinetic modelling tools for oxide growth such as DICTRA [38] and help to explain the very rapid corrosion rates observed in field studies performed in biomass- and waste fired boilers [39,40].

Table 1
Nominal composition (wt%) of Fe-2.25Cr-1Mo [48].

Fe	Cr	Mo	Mn	Si	C	P	S
Bal.	1.9–2.6	0.87–1.13	0.3–0.6	≤0.50	0.05–0.15	< 0.025	< 0.025

2. Experimental procedure

2.1. Sample preparation

The investigated alloy is an Fe-2.25Cr-1Mo steel (see Table 1 for chemical composition). Prior to exposure the steel was cut into coupons (tube furnace exposures: 15 × 15 × 2 mm, TGA: 10 × 8 × 2 mm), ground with SiC (grit size P320), a Largo disc (9 µm) and polished with diamond suspension (3 and 1 µm) until mirror like appearance. The polished steel coupons were degreased and cleaned in acetone and ethanol by using ultrasonic agitation. Both non-coated and KCl(s) coated steel coupons were investigated. KCl(s) was deposited on the coupons before exposure by spraying a solution of KCl (0.1 mg/cm^2) solved in ethanol and water (80:20) and subsequently dried in cool air. All samples were stored in a desiccator (drying agent P_2O_5) prior to exposure and awaiting analysis to avoid atmospheric corrosion and hygroscopic effects of chlorine containing species.

2.2. Exposures

The exposures were performed in an isothermal horizontal tube furnace as well as a vertical furnace system for recording the oxidation kinetics by thermogravimetric analysis (TGA). The samples were positioned parallel to the direction of the gas flow and all parts of the systems were kept above the dew point of water to prevent condensation. The reference exposure gas consisted of 20%H_2O + 5%O_2 + 75% N_2. The exposures were carried out at 400 °C for 24 h on both non-coated and KCl(s) coated steel coupons. The exposures in the horizontal tube furnace were made with three samples positioned in a sintered alumina holder during each exposure. The TGA exposures were performed with a single sample at the time, but several exposures were made to ensure reproducibility. The oxidation kinetics were recorded using a Setaram Setsys thermobalance (flow rate of 15 ml/min) humidified with a Setaram Wetsys.

2.3. Analytical techniques

2.3.1. Scanning electron microscopy (SEM)

Surface and cross-sectional characterisation of the samples were performed by an FEI Quanta ESEM 200 and a Zeiss LEO Ultra 55 FEG SEM, both equipped with a field emission gun and a detector for Energy dispersive X-ray spectroscopy (EDX). The microscopes were operated in high vacuum mode with accelerating voltages between 15–20 keV for the chemical analysis, 1.5–2 keV for surface sensitive imaging in the Zeiss LEO Ultra 55 FEG SEM and 10–20 keV for imaging in the FEI Quanta ESEM 200. Both secondary electrons (SEs) and backscattered electrons (BSEs) were used for imaging.

2.3.2. Broad ion beam (BIB)

Wide cross sections of the samples were prepared by Broad ion beam (BIB) milling. The BIB used in this study is a Leica EM TIC 3X BIB with a triple Ar ion gun operated at 6.5 kV. Prior to milling the samples were prepared by application of a 0.5 mm thick silicon wafer glued to the sample with Loctite® 415. The samples were thereafter cut prior to milling by a low speed saw without lubrication. The Si-wafer was used as a protection for the oxide to stay intact during cutting as well as for beam damage during ion milling.

2.3.3. Focused ion beam (FIB)

Site specific cross sections for TEM analysis were prepared using an FEI Versa3D LoVac DualBeam. The instrument is a combined FIB/SEM, equipped with a Ga liquid ion metal source (LMIS), a Gas Injection System for deposition of Pt (used as a protective cap layer to reduce beam damage and ion implantation) and an Omniprobe needle for lift-out of thin TEM lamellae. The instrument was operated in high vacuum mode at 30 keV, with varying beam currents (30 pA–15 nA) throughout the lift-out procedure. The FIB was also used for imaging the BIB-milled cross sections with ion induced secondary electrons (iSEs) at 30 keV and 10 pA for enhanced grain contrast to measure the grain size of the oxides. The grain sizes were measured in two dimensions assuming that the most relevant direction for grain boundary diffusion is the growth direction represented in the two-dimensional cross sections.

2.3.4. Transmission electron microscopy (TEM)

Cross sections of the oxides were investigated in further detail using an FEI Titan 80-300 TEM equipped with an Oxford X-sight EDX detector for chemical analysis. The microscope was operated in Scanning TEM mode (STEM), at an accelerating voltage of 300 keV. Both bright field (BF) and High Angle Annular Dark field (HAADF) imaging modes were used. The quantification of oxygen from the STEM/EDX analysis is not reported in this paper due to large errors associated with oxygen quantification in EDX analysis. Instead the cationic percent is reported (in at%) assuming stoichiometric oxides.

2.3.5. X-ray diffraction (XRD)

The crystalline oxide phases formed on the samples were characterised by a Siemens D5000 powder X-ray diffractometer with a CuK_α source ($\lambda = 1.5418$ Å). The instrument was operated in grazing incidence geometry with an angle of incidence of 2–4° and a measuring range of $10° < 2\theta < 85°$.

2.3.6. Transmission Kikuchi diffraction (TKD)

Transmission Kikuchi diffraction (TKD) was used in order to locally characterise some of the phases of the oxide scale. The instrument used for the TKD measurements was a Tescan GAIA3 equipped with a NordlysNano Camera for electron backscatter diffraction (EBSD) analysis. The instrument was operated at 30 keV and the FIB-milled thin foil was mounted in a tilted holder at 20° to maintain the Kikuchi diffraction patterns and locally distinguish between corundum and spinel type oxides.

3. Results

The results below show the influence of KCl on oxidation of a low alloyed steel at 400 °C both regarding oxidation kinetics, oxide morphology and scale microstructure by the comparison of a reference exposed sample as well as a KCl exposed sample.

3.1. Oxidation kinetics

3.1.1. $O_2 + H_2O$ (reference)

The TGA performed on the reference sample showed slow parabolic kinetics ($k_p = 7.3 \times 10^{-14}\,g^2\,cm^{-4}\,s^{-1}$) resulting in a low mass gain (~0.1 mg/cm^2) after 24 h (see Fig. 1). The oxide thickness was estimated to 0.6 µm from mass gain data. The calculation was performed by assuming that the scale consisted of dense Fe_3O_4 and that all mass gain was related to oxygen uptake from the exposure atmosphere [41].

3.1.2. $O_2 + H_2O + KCl(s)$

The KCl(s) coated sample grew with repeated rapid parabolic kinetics resulting in a high mass gain (~0.9 mg/cm^2) after 24 h (see Fig. 1). The growth was parabolic with the parabolic rate constant $k_{p,1} = 4.3 \times 10^{-12}\,g^2\,cm^{-4}\,s^{-1}$ for the first 12 h and thereafter disrupted by a short linear growth period followed another rapid parabolic growth ($k_{p,2} = 3.2 \times 10^{-12}\,g^2\,cm^{-4}\,s^{-1}$). The kinetic transition was, between the first and second parabolic growth, was not always as sharp as shown in Fig. 1 and the time for the kinetic transition varied between samples. However, the kinetic transition occurred at a calculated thickness of at least 3 µm and the final mass gains after 24 h were similar for all samples. The oxide thickness was estimated from mass gain data to 6.5 µm in total, corresponding to 4.2 µm before the kinetic transition (0–12 h) and 2.3 µm after (12–24 h).

3.2. Oxide scale

3.2.1. $O_2 + H_2O$ (reference)

3.2.1.1. Surface morphology. The surface morphology of the reference sample was homogeneous and consisted of blade like whiskers covering all the sample surface (see Fig. 2a, b). The blades were about 30 nm in thickness, 200 nm wide and approximately 0.5–1 µm long. No signs of crack formation nor large variations in thickness were observed on the surface. Both corundum (Fe_2O_3) and spinel (Fe_3O_4) type oxides were detected by XRD (see Fig. 7).

3.2.1.2. Scale microstructure. The oxide scale formed on the reference sample was thin and well-adherent with a uniform thickness of approximately 0.5 µm (see Fig. 3). The scale was multi-layered and composed of a thin outward growing hematite (Fe_2O_3) layer on top of a thicker outward growing magnetite (Fe_3O_4) and a thin inward growing mixed chromium containing spinel ($(Fe,Cr)_3O_4$) at the scale/metal interface. The corundum (Fe_2O_3) and spinel ($(Fe_x,Cr_{1-x})_3O_4$) type oxides were detected by XRD (see Fig. 7) and the composition determined by STEM/EDX analysis of a representative region (see Fig. 3b–d). The STEM/EDX analysis showed that both the outward growing oxides were pure iron oxides while the inward growing spinel contained an average of 10 at% Cr (6.5–19 at%), 2 at% Si (1–4 at%), 1–2 at% Mo, with iron in balance, excluding oxygen from the quantification (see Fig. 3).

The boundary between inward and outward growing oxides, i.e. the original metal surface, was determined from microstructure and the presence of chromium in the inward growing spinel (see the STEM/EDX linescan for chromium in Fig. 3d). The distribution of oxides in the multi-layered scale was approximately 25% Fe_2O_3, 50% Fe_3O_4 and 25% mixed spinel, resulting in an oxide scale consisting of 25% inward growing and 75% outward growing oxide (see Table 2). No depletion zone of chromium was observed in the alloy after 24 h of exposure. A mass balance calculation was performed from the STEM/EDX data indicating that no substantial amount of any alloying element was lost by evaporation or spallation.

The oxide grains in the Fe_3O_4 layer were columnar with an average grain size of 140 nm × 270 nm (aspect ratio of 0.5) while the grains of the Fe_2O_3 layer were more equiaxed (aspect ratio 0.7) and approximately 75 nm × 110 nm in size (see Fig. 3b).

3.2.2. $O_2 + H_2O + KCl(s)$

3.2.2.1. Surface morphology. The surface morphology of the oxide scale formed on the KCl(s) coated sample was heterogeneous (see Fig. 4a, b). The surface contained a noticeable amount of remaining, partly unreacted KCl crystals and a variety of oxide morphologies. The remaining KCl crystals covered nearly 20% of the total surface area, both present as isolated crystals and larger crystal agglomerates (see Fig. 4a). A considerable number of the crystals were completely overgrown by iron oxide. Both the corundum (Fe_2O_3), spinel (Fe_3O_4) and rock salt (KCl) phases were detected by XRD (see Fig. 7). The XRD results also indicated the presence of maghemite (γ-Fe_2O_3) which has the same crystal structure as magnetite (Fe_3O_4) but the chemical formula of hematite (Fe_2O_3). The base oxide (i.e. the most common type of oxide region in between the remaining KCl crystals) had a granular surface morphology with a granule diameter of approximately 0.5–1 µm (see Fig. 4b). In contrast to the reference sample the plan view

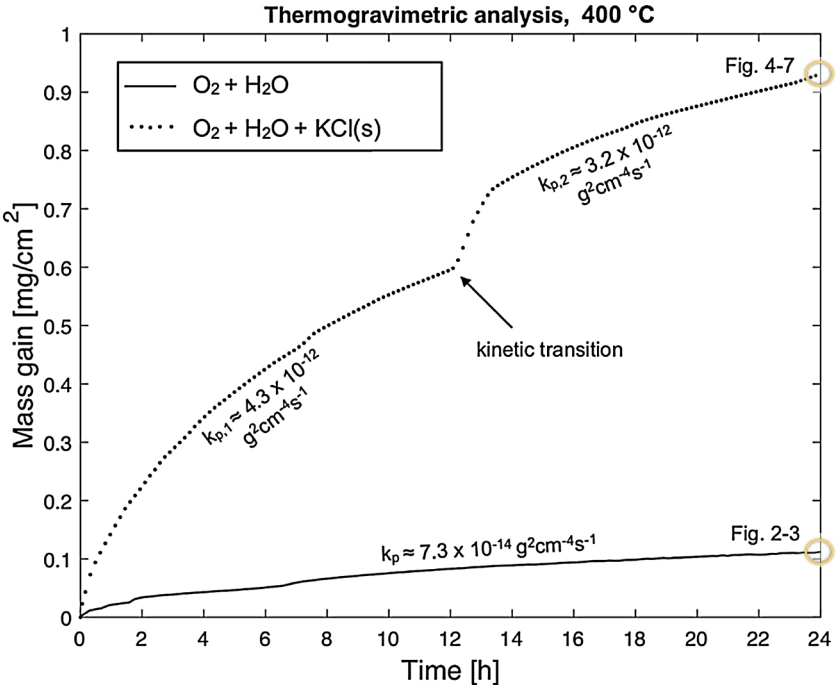

Fig. 1. Thermogravimetric analysis showing the oxidation kinetics of Fe-2.25Cr-1Mo exposed at 400 °C for up to 24 h for both non-coated (reference) and KCl(s) coated steel coupons. Both the reference and KCl(s) coated samples show parabolic kinetics but with different parabolic rate constants. The parabolic rate constants, $k_{p,i}$, marked in the figure, are calculated from $\Delta m^2 = 2k_{p,i}t$, where Δm represent the mass change (y-axis) and t = time (x-axis). A kinetic transition is observed in the curve for the KCl(s) coated sample, with similar parabolic rate constants before and after the transition.

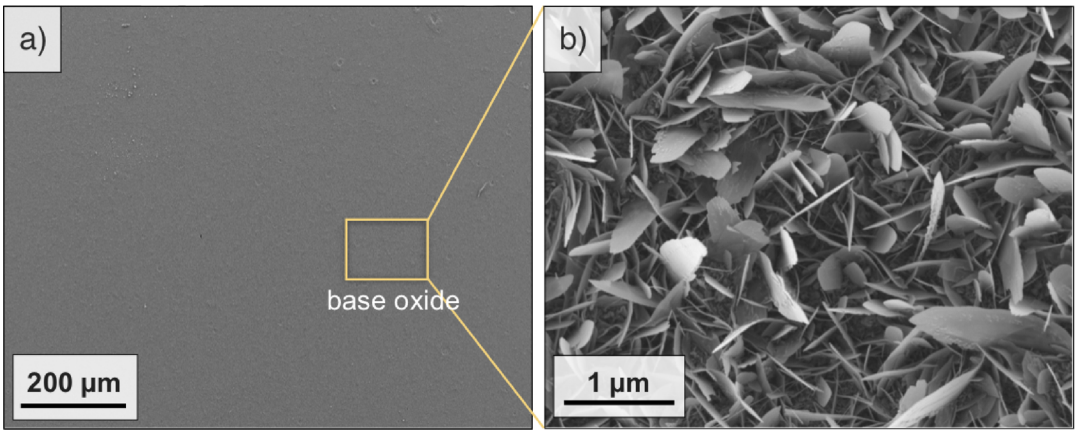

Fig. 2. Surface morphology of the base oxide formed on a non-coated (reference) Fe-2.25Cr-1Mo steel after 24 h exposure in 5%O_2 + 20%H_2O + 75%N_2 at 400 °C. The surface morphology of the reference sample is homogeneous and structured in blade like whiskers covering all the sample surface (a, b). The plan view images are produced by secondary electrons at an acceleration voltage of 10 keV (EHT detector) and 2 keV (in-lens detector) respectively. The microstructure of the base oxide, marked in (a), is analysed in further detail (see Fig. 3).

investigation showed that cracks formed on the sample surface (see Fig. 4a). Some cracks were partly overgrown by oxide (see Fig. 5a, b). A one-sided cross section (see Fig. 5c, d), ion milled through a crack, showed the formation of two subscales detached completely to form a new subsurface, covered by whiskers, below the upper subscale.

3.2.2.2. Scale microstructure. The base oxide (in between the KCl particles) formed on the KCl(s) coated sample was thick and partly delaminated (see Fig. 6a). The scale consisted of two delaminated, multi-layered oxide subscales with a total thickness of 5.5–7.3 µm (average 6.4 µm) (see Fig. 6b). The upper subscale had an average thickness of 4.6 µm while the lower subscale was approximately 1.8 µm. The upper subscale, was measured on several regions on different samples and concluded to be at least approximately 3.5 µm while no delamination was observed in regions where the oxide was measured to be thinner. The multi-layered subscales were interpreted as composed of a thin, outward growing Fe_2O_3 layer on top of a thicker outward growing Fe_3O_4 and an inward growing mixed (Fe, Cr, Mo, Si)-spinel at the bottom (see Fig. 6b–e). As mentioned above, the XRD results indicated both hematite (Fe_2O_3), spinel/magnetite and maghemite(γ-Fe_2O_3)). The maghemite was however not confirmed by TEM or TK. The STEM/EDX linescan for chromium (see Fig. 6d, e) was used for identification of the inward and outward growing oxides. No depletion zone of chromium was observed in the alloy after 24 h of exposure and no chlorine was detected in the upper subscale. A mass balance calculation performed from the STEM/EDX data indicated that no substantial amount of any alloying element was lost by evaporation or spallation.

The upper subscale was concluded to consist of 10% outward growing Fe_2O_3 (plus 10% incorporated in the Fe_3O_4), 50% outward growing Fe_3O_4 and 30% inward growing (Fe,Cr)-spinel ($(Fe,Cr)_3O_4$) (see Table 3) based on data from XRD and EDX analysis as well as the oxide microstructure. The STEM/EDX analysis (see Fig. 6d, e) showed that the outward growing oxides consisted of pure iron oxide with small traces of potassium (< 1%) in the top layers of the upper outward growing scale (Fe_2O_3 + Fe_3O_4) (see Fig. 6d, e). The inward growing spinel in the

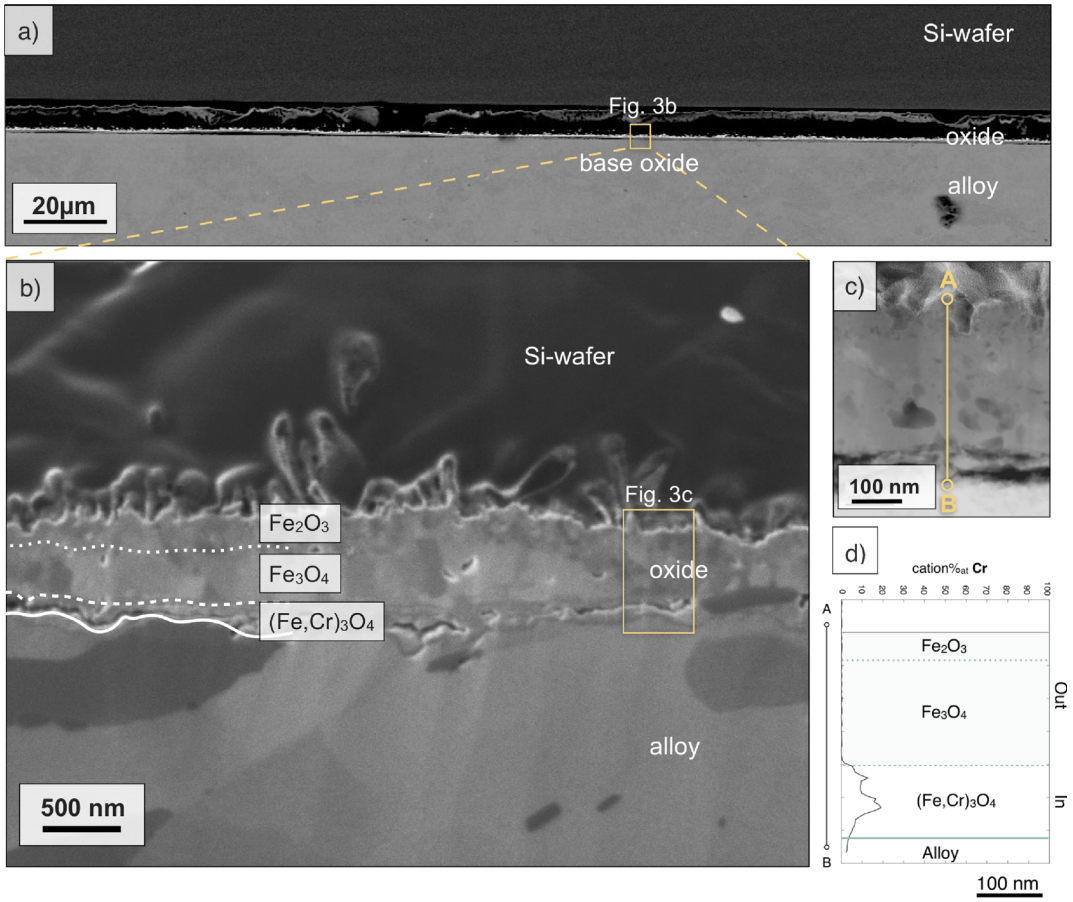

Fig. 3. (a, b) Cross sectional views of the oxide scale formed on Fe-2.25Cr-1Mo steel exposed in reference conditions ($5\%O_2$ + $20\%H_2O$ + $75\%N_2$) for 24 h at 400 °C. The scale is thin and well-adherent with a uniform thickness of 0.5 µm. The cross section is prepared by BIB milling and imaged with (a) backscattered electrons at an acceleration voltage of 10 keV and (b) ion induced secondary electrons (iSE) at 30 keV and 10 pA. (c) HAADF-STEM image of a FIB milled TEM lamella showing the position of the STEM/EDX linescan (d) (see marking A-B). The STEM/EDX analysis shows that the scale is layered with a duplex outward growing scale (Fe_2O_3 + Fe_3O_4) and an inward growing chromium containing spinel ($(Fe,Cr)_3O_4$) at the scale/metal interface. (d) The STEM/EDX linescan for Cr, which is used as a marker for the original metal surface and the interface between inward and outward growing oxides.

upper subscale contained an average of 7 at% Cr (2.5–10%), 1 at% Si (1–2%), < 1 at% Mo, with iron in balance, excluding oxygen from the quantification. The TKD results confirmed that the top oxide layer contained hematite Fe_2O_3 (corundum), with an average grain size of 190 nm × 330 nm (aspect ratio ≈ 0.6), (see blue regions in Fig. 6c). The thicker oxide below was confirmed to be spinel/magnetite (see yellow regions in Fig. 6c) with columnar oxide grains of average grain size 230 nm × 780 nm (aspect ratio ≈ 0.3). The brighter contrast in the SE image in Fig. 6b appeared to match the indexed corundum in the TKD mapping (see blue regions in Fig. 6c). The SE image in Fig. 6b also showed a band below the pores in the upper subscale with brighter contrast than the surrounding oxide. The difference in contrast in combination with the TKD results indicated that this band was Fe_2O_3 (average grain size 280 nm × 500 nm) as well as local regions in the mixed (Fe, Cr, Mo, Si)-spinel layer below (see Fig. 6c). However, due to the small area analysed in the TKD, we cannot conclude, but only speculate in, that all brighter regions observed in Fig. 6b were Fe_2O_3 (corundum).

The lower subscale was concluded to consist of 10% Fe_2O_3, 45% Fe_3O_4 and 45% (Fe,Cr)-oxide (including the fibre structured oxide (35% $(Fe,Cr)_xO_y$) (see Table 3) based on data from XRD and EDX analysis as well as the oxide microstructure. The STEM/EDX analysis showed an outward growing pure iron oxide and a mixed inward growing oxide. The oxide grains of the Fe_3O_4 layer in the lower subscale were 260 nm × 700 nm (aspect ratio ≈ 0.4) while the grains in the top oxide layer (Fe_2O_3) of the lower subscale were equiaxed with an average grain size of approximately 80 nm (see Fig. 6b). This layer was concluded to be Fe_2O_3 due to the visible contrast in the SE image, the smaller grain size of this oxide layer and the whiskers formation, characteristic for Fe_2O_3 in exposure to H_2O, as reported in several studies [17,29,34] (see Fig. 6b).

Table 2
Summary of the oxide scale formed on the reference exposed (O_2 + H_2O + N_2) sample.

Reference	Thickness (estimated[a]) [µm]	Thickness (measured) [µm]	Relative amount (%)	Growth direction	In (%)	Out (%)
Fe_2O_3	–	0.13	25	Out	–	–
Fe_3O_4	–	0.26	50	Out	–	–
$(Fe,Cr)_3O_4$	–	0.13	25	In	–	–
Total	0.6	0.5	100	–	25	75

[a] Calculated from mass gain.

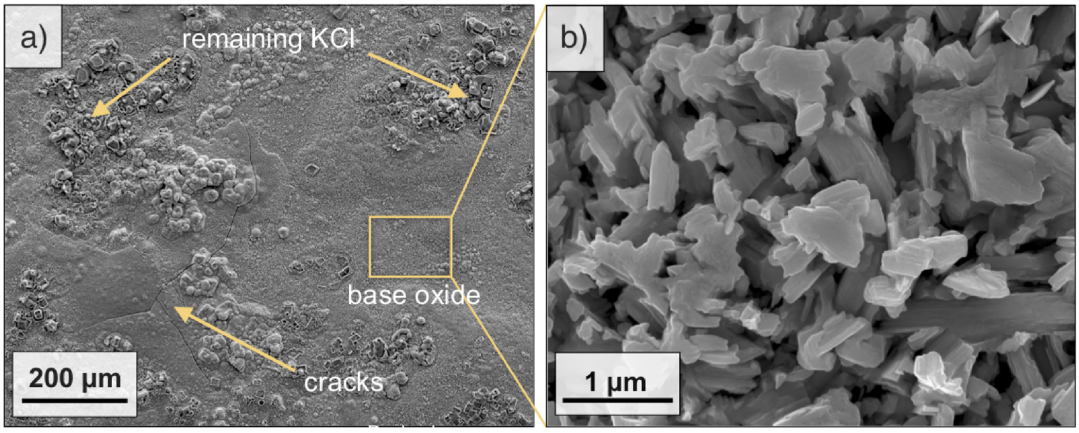

Fig. 4. Surface morphology of the base oxide formed on a KCl(s) coated Fe-2.25Cr-1Mo steel after 24 h exposure in 5%O_2 + 20%H_2O + 75%N_2 at 400 °C at low (a) and high (b) magnification. The surface morphology is heterogeneous with partly consumed and overgrown KCl(s) crystals still remaining on the sample surface. Crack formation is observed on the sample surface (see Fig. 5 for more details). The base oxide (in between the remaining KCl crystals) is heterogeneous but is mainly structured in a granular surface morphology. The plan view images are produced by secondary electrons at an acceleration voltage of 20 keV (a) and 10 keV (b). The microstructure of the base oxide marked in figure (a), is analysed in further detail (see Fig. 6).

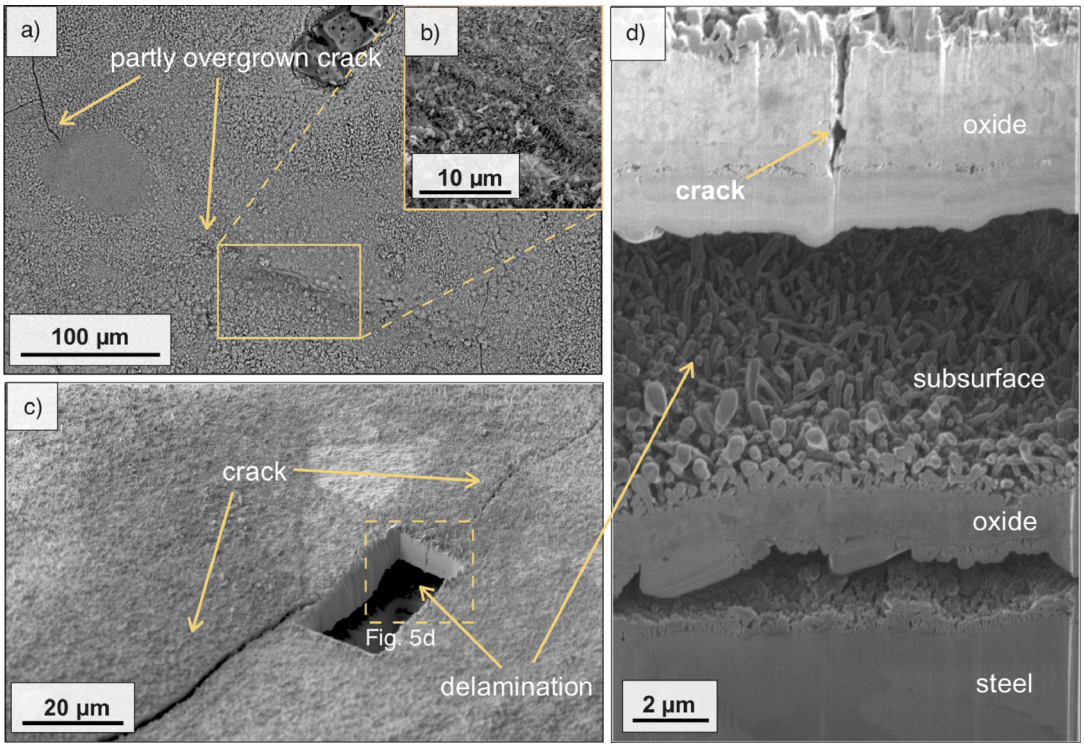

Fig. 5. SEM/FIB images showing crack formation of the oxide scale formed on a KCl(s) coated Fe-2.25Cr-1Mo after 24 h exposure at 400 °C in 5%O_2 + 20% H_2O + 75%N_2. (a) BSE image of the oxidised surface showing a partly overgrown crack. (b) SE image showing the overgrown crack at higher magnification. (c) SE images of a FIB-milled cross section through a crack formed on the oxide surface. The oxide scale is delaminated and a new subscale has formed underneath the detached oxide scale (d). The surface crack goes all through the top scale to the new subsurface where whiskers have formed (d). Note that the image in (b) is taken with ion induced secondary electrons (iSEs) at a tilt angle of 52°. Hence the vertical measurements should be corrected for (x = µm/sin(52°)).

The inward growing oxide could be divided into two different types, separated by a lateral gap. The oxide above this lower gap was suggested to be a dense spinel oxide ($(Fe,Cr)_3O_4$) while the oxide at the scale metal interface showed a characteristic fibre like microstructure noticeably different from the rest of the oxide scale (see Fig. 6b). Diffraction in TEM (not shown) indicated that this oxide was crystalline showing a spot diffraction pattern in the TEM. However, the diffraction pattern was not recorded and indexed why it cannot be concluded with certainty. The XRD data did only detect Fe_2O_3(corundum), $(Fe_{1-x},Cr_x)_3O_4$ (spinel) and the alloy (BCC) why it is proposed that the phase is spinel if crystalline. The dense inward growing spinel in the lower subscale contained approximately 3–5 at% Cr with iron in balance and traces of silicon (< 1 at%) and chlorine (< 1 at%) while the fibre like oxide ($(Fe,Cr)_xO_y$) layer, at the scale/metal interface, contained approximately 20 at% Cr (16–21 at%), 3 at% of Mo (2–3 at%), 4 at% Si (4–6 at%) with iron in balance and traces of chlorine (< 1 at%). It should be noted that the porous microstructure made the quantification of this region difficult, why the quantification of this region should be considered as approximate. In addition, since both molybdenum and chlorine were detected in this oxide, there is a risk of overlapping X-ray energies of the K-peaks of chlorine and L-peak family of Mo, which makes the quantification of small amounts of chlorine troublesome.

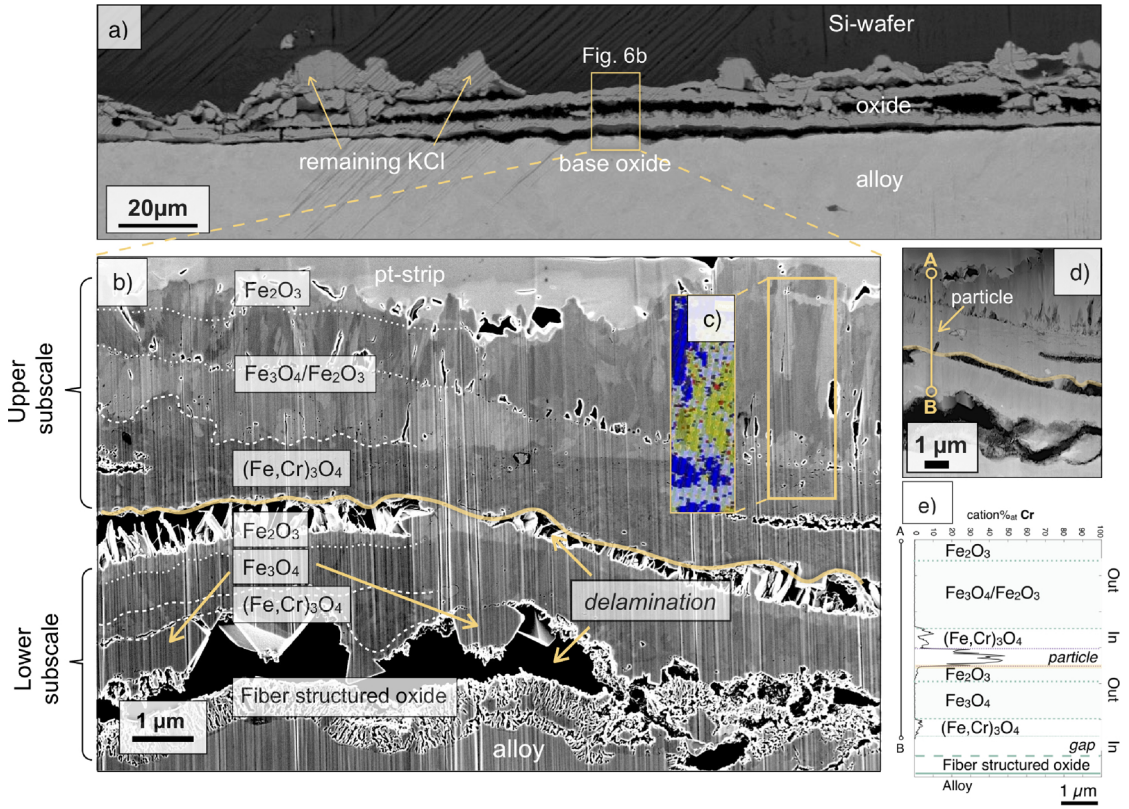

Fig. 6. (a) BSE image showing the cross section of the oxide formed on the KCl(s) coated Fe-2.25Cr-1Mo steel exposed for 24 h at 400 °C. The cross section is prepared by BIB milling and imaged at an acceleration voltage of 10 keV. (b) A SE image of a TEM lamella prepared by FIB and imaged at an acceleration voltage of 1.5 keV. The scale appear to have formed in two growth stages, forming two multi-layered oxide subscales, consisting of outward growing Fe_2O_3, Fe_3O_4 and an inward growing chromium containing oxide ($(Fe,Cr)_2O_3$). The phases of the upper subscale are characterised by TKD (c) represented in (c) as blue for corundum (Fe_2O_3) and yellow for spinel (Fe_3O_4). (d) HAADF-STEM image showing the position of the STEM/EDX linescan (see line marking A-B). (e) STEM/EDX linescan for Cr showing the presence of Cr in two oxide layers in the scale. The Cr-peak in the middle is due to an Fe-Cr-Mo-K-Cl containing oxide particle in the middle of the scale, not representative for this type of sample, why it will not be discussed in further detail in this paper. The presence of Cr is used as a marker for the original metal surface, i.e. the interface between inward and outward growing oxide. (For interpretation of the references to colour in this figure legend, the reader is referred to the web version of this article.)

4. Discussion

The present study focuses on the initial stages of the KCl-induced corrosion of Fe-2.25Cr-1Mo at 400 °C. The study includes a detailed microstructural investigation of the base oxide scale in combination with in-situ mass gain kinetics.

It is well known that alkali chlorides and other chlorine containing compounds cause accelerated corrosion of both pure iron [3–7], stainless steels [2–5,7–20] and low alloyed steels [2,5,4,8,10,11,13,21–26]. Nevertheless, the microstructure and the composition of the oxide scales grown on low alloyed steels in presence of KCl(s) have not been investigated in detail and the corrosion mechanism of both chlorine and alkali species are still under debate. Previous studies on Fe-2.25Cr-1Mo [24–26] have shown indications of cracked and/or delaminated oxide scales in presence of KCl(s). However, the mechanisms and influence on the total growth process are not well understood. The present study

Table 3
Summary of the oxide scale formed on the KCl(s) coated sample (O_2 + H_2O + N_2 + KCl(s)).

KCl(s)	Thickness (estimated[a]) [µm]	Thickness (measured) [µm]	Relative amount	Growth direction	In (%)	Out (%)
Upper subscale						
Fe_2O_3	–	0.5	10	Out	–	–
Fe_3O_4/Fe_2O_3	–	2.6	60	Out	–	–
$(Fe,Cr,M)_3O_4$	–	1.5	30	In	–	–
Total	4.2	4.6	100	–	30	70
Lower subscale						
Fe_2O_3	–	0.2	10	Out	–	–
Fe_3O_4	–	0.8	45	Out	–	–
$(Fe,Cr)_3O_4$	–	0.2	10	In	–	–
$(Fe,Cr,M)_xO_y$ (fibre)	–	0.6	35	In	–	–
Total	2.3	1.8	100	–	45	55
Full scale	6.5	6.4	100	–	35	65

[a] Calculated from mass gain.

focuses on how the presence of KCl(s) influences the growth kinetics and microstructure of the oxide scale formed on a low alloyed steel at 400 °C and how the microstructural changes may affect the growth process.

4.1. Oxidation of Fe-2.25Cr-1Mo

The present study shows that the oxide scale formed on Fe-2.25Cr-1Mo in absence of KCl(s) (reference sample) is thin and well-adherent with no indications of scale cracking (see Figs. 2 and 3), corresponding well with previous studies on the initiation of corrosion of low alloyed steels and iron in presence of H_2O [24,33,34]. The thickness is uniform and in good agreement with the average thickness calculated from mass gain data indicating that no noticeable amount of any species has been lost by spallation or evaporation during exposure (see Table 2). The mass balance performed from STEM/EDX data resulted in the same conclusion.

The slow parabolic kinetics recorded by TGA (see Fig. 1) indicates that the oxide growth is diffusion controlled in good agreement with previous studies [24,25,35]. The parabolic rate constant ($k_{p,Ref} = 7.3 \times 10^{-14} g^2\,cm^{-4}\,s^{-1}$) is in the same range as previously reported for low alloyed steels in presence of water vapour at 400 °C and 1–2 order of magnitudes lower than pure iron in similar exposure conditions [24,25,32,34]. The difference in parabolic rate constant between iron and Fe-2.25Cr-1Mo observed in this study indicates that the presence of chromium, detected in the inward growing spinel, has an important influence on the overall growth rate at 400 °C.

The multi-layered type of oxide scale observed in this study (see Fig. 3) is in good agreement with previous studies performed on low alloyed steel and iron [10,17,25,32,34,35]. The oxide distribution in this oxide scale is concluded to be approximately 25% inward growing and 75% outward growing oxide (see Table 2). The STEM/EDX results show that the mixed inward growing spinel has higher relative levels of Cr, Si and Mo (compared to the original alloy composition. This is proposed to be explained by the rapid outward diffusion of iron to grow the Fe_2O_3 and Fe_3O_4, while chromium remains at its original position due to the relatively slow diffusivity of Cr^{3+} ions in the spinel phase [36,37].

4.2. Influence of KCl

The present study clearly shows that KCl(s) accelerates and influences the growth process of the oxide scale formed on Fe-2.25Cr-1Mo. Both oxidation kinetics, thickness, surface morphology and microstructure of the base oxide scale changes markedly when KCl(s) is present. In contrast to the reference sample the oxide scale is thick, heterogeneous and decohesive and shows formation of several cracks on the sample surface in good agreement with previous studies on low alloyed steel in presence of KCl(s) at 400 °C [24–26] or HCl(g) at higher temperatures [13]. The oxide scale is formed by two delaminated multi-layered subscales, composed of Fe_2O_3, Fe_3O_4 and $(Fe,Cr,Si,Mo)_3O_4$. Uusitalo et al. [10] observed a similar, but thicker, microstructure of the oxide scale formed on Fe-2.25Cr-1Mo exposed for 1000 h at 550 °C in 500 vppm HCl (g) + 20%H_2O + 14%CO_2 + 3%O_2 + Ar (bal.). It should be noted that those exposures were interrupted and samples weighted every 100 h, which could result in delimitation of the oxide scale.

4.2.1. Oxide growth

Both the microstructural investigation and oxidation kinetics indicate that the scale growth is diffusion controlled (see Fig. 1). However, the kinetic transition observed suggests that the total growth process of the oxide scale is strongly influenced by microstructural changes during growth. The growth rate is markedly higher compared to the reference sample ($k_{p,KCl} \approx 45–60 \times k_{p,Ref}$), supporting that the diffusion rate through the scale is strongly influenced by addition of KCl(s).

The oxidation kinetics are parabolic both before and after the kinetic transition, suggesting that the growth of each subscale is diffusion controlled. However, the parabolic rate constants before and after the kinetic transition ($k_{p,1} = 4.3 \times 10^{-12}$ $g^2\,cm^{-4}\,s^{-1}$ and $k_{p,2} = 3.2 \times 10^{-12}$ $g^2\,cm^{-4}\,s^{-1}$) are in the same order of magnitude indicating that the first formed oxide does not hinder the diffusing species noticeably (see Fig. 1). Thus, the oxide scale can grow in a repeated parabolic process. The lower value of the parabolic rate constant for the second subscale is proposed to be caused by that not all the surface oxidises simultaneously below the delaminated subscale. The estimated thicknesses, based on the mass gain before (0–12 h) and after (12–24 h) the kinetic transition, provided an estimated thickness of 4.2 μm and 2.3 μm respectively resulting in a total estimated thickness of 6.5 μm. The calculated thicknesses correspond well with the measured thickness of the upper (0–12 h) and lower (12–24 h) subscales as well as the total thickness of the scale (see Table 3). These results suggests that the growth of each subscale is represented by the TG curve before and after the kinetic transition. The results also indicate that the main corrosion product formed is oxide and that evaporation of KCl(s) on Fe-2.25Cr-1Mo exposed at 400 °C is low, as reported by Folkeson et al. [24]. The microstructural investigation concludes that the presence of KCl(s) makes the oxide scale susceptible to crack formation and delamination, suggested to explain the global kinetic transition observed in the TG curve (see Fig. 1).

The oxide formed in presence of KCl(s) shows rapid diffusion throughout all of the exposure and no indications of incubation time. Olivas Ogaz et al. [27] showed that Fe-2.25Cr-1Mo exposed under similar conditions at 400 °C, but on pre-oxidised samples, had a slight incubation time before the rapid kinetics started. Grabke et al. [8] did however not see much incubation time on pre-exposed Fe-2.25Cr-1Mo, exposed to NaCl at 500 °C. The deposited KCl in this study is in contact with the metal from the beginning (no pre-oxidation) and proposed to spread rapidly on the surface as a eutectic melt as proposed by Jonsson et al. [25]. This could explain the instant acceleration of KCl as is observed in this study.

Moreover, the grain morphology of the Fe_3O_4 layers, of both the upper and lower subscale, correspond well with what has previously been reported for iron oxide at around 400 °C while the top Fe_2O_3 layer (upper subscale) has larger oxide grains compared to previous studies [32,34,42]. However, the grain size of both Fe_2O_3 and Fe_3O_4 has increased compared to the reference sample, i.e. the number of grain boundaries has decreased. More grain boundaries are often attributed to increased growth rate of iron oxide at moderate temperatures caused by faster ionic transport through the grain boundaries compared to bulk diffusion [29,34]. This observation therefore indicates that the presence of KCl(s) changes the diffusion rate of ions through the oxide, possibly by lowering the activation energy for diffusion through the bulk and/or grain boundaries, since the number of grain boundaries does not increase.

Traces of potassium (< 1 at%) were detected in the top oxide layers of the outer subscale (both in what is proposed to be the top Fe_2O_3 and in the Fe_3O_4 layer). The small amounts of potassium detected may possibly change the conditions for diffusion through this oxide. Jiang et al. [43] proposed that the presence of potassium on iron oxide surfaces could promote the reduction of Fe^{3+} to Fe^{2+}, which in turn could alter the properties of the oxide scale. This has not been investigated in any detail in this study but could possibly explain the increased relative amount of inward growing scale observed. In this study the phase of the potassium compound is not determined. Previous studies have suggested the formation of $KFeO_2$, K_2O or KOH on Fe_2O_3 since this would be energetically favourable under similar exposure conditions [24–26,30]. However, none of these phases have been detected. Further investigations are ongoing to investigate how potassium is positioned in the oxide, in what phase it is present and how it may influence the bulk and/or grain boundary diffusion.

4.2.2. Crack formation and delamination

In this study both cracks and delamination are observed on the KCl (s) coated sample, in good agreement with previous studies [10,24,26,31]. A cracked and/or delaminated oxide scale would affect

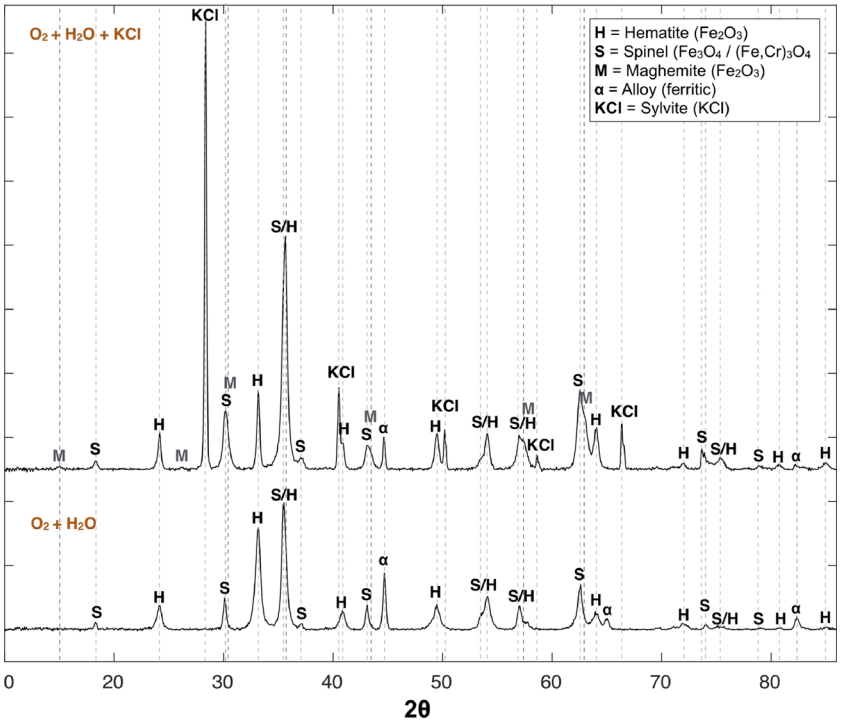

Fig. 7. X-ray diffractogram of Fe-2.25Cr-1Mo exposed at 400 °C in 5%O_2 + 20%H_2O + 75%N_2 for 24 h in absence (lower diffractogram) and presence (upper diffractogram) of KCl(s). The diffractograms suggests that corundum and spinel type oxides are present on the surface after both exposures, interpreted as hematite (Fe_2O_3) and magnetite/mixed spinel (M_3O_4). The diffractogram also detects remaining KCl(s) on the sample exposed in presence of KCl(s) and indications of maghemite (γ-Fe_2O_3), having a spinel type crystal structure, but the same chemical formula as hematite.

the corrosion rate extensively by changing the conditions for diffusion through the oxide scale. Cracks would serve as local highways for the corrosive atmosphere through the scale and delamination would result in the formation of a new reactive surface. Together these two microstructural phenomena could result in a global change in conditions and a sharp kinetic transition. This is supported by the plan view and cross section investigation showing that the base oxide is decohesive on the KCl(s) coated sample and that cracks form in contrast to the reference sample. From this investigation we propose a growth process that includes the delamination and subsequent crack formation as critical parts of the explanation to the microstructural changes and kinetic transitions observed in the TGA. The complete growth process proposed is schematically described in Fig. 8. The process starts with a rapid spread of KCl(s) over the sample surface, explaining the instantly high growth rate observed in the TGA, with subsequent growth of a multi-layered oxide scale (upper subscale). The scale grows relatively thick (3.5–5 μm) during the first few hours and then partly delaminates to form a lateral gap and a new reactive surface. The oxide scale cracks at local positions which allows for the oxidising atmosphere to enter and rapidly spread through the lateral gap. The inflow of the oxidising atmosphere subsequently results in new environmental conditions, allowing for a new subscale (lower subscale) to form below the delaminated scale. This results in a global kinetic transition and the beginning of a new growth cycle (see Fig. 1).

In experimental studies it is normally challenging to determine whether observed cracks or delamination are parts of the growth process or if they are formed post exposure during the cooling process or sample preparation. However, in this study some of the cracks were partly overgrown by oxide indicating that the cracks had formed during growth (see Fig. 5a, b). Also, a new subsurface consisting of Fe_2O_3 had formed under the first formed subscale (upper gap, see Fig. 5c, d) and pure Fe_3O_4 crystals had grown in the lower gap (see Fig. 6). Formation of Fe_2O_3 in the middle of the scale is not thermodynamically expected in a dense oxide where we have a gradient in oxygen partial pressure explaining the multi-layered scale. Hence, the uniform layer of Fe_2O_3 observed in the middle of the scale strongly indicates that the oxygen partial pressure has increased above the dissociation pressure of Fe_3O_4 ($pO_2 > 10^{-22}$ atm at 400 °C [29]) to support the transformation of Fe_3O_4 to Fe_2O_3. This may be explained by delamination in combination with crack formation during growth.

An obvious question that rises is also whether the cracks form as a consequence of delamination or if the delamination caused the crack formation. However, if the cracks formed before the scale detached, we should have a local corrosion attack in the vicinity of the cracks, which is not observed in this study. This suggests that delamination occurred before scale cracking. Also, local acceleration of corrosion would not result in a global kinetic transition as observed in the TGA (see Fig. 1). Hence, scale cracking is proposed to occur after, possibly caused by, the delamination.

Possible explanations to the delamination could be growth stresses, accumulation of vacancies at the decohesive interfaces or formation of metal chlorides. Jonsson et al. [25] observed spallation on Fe-2.25Cr-1Mo in exposure to KCl(s) at 400 °C. The spallation was suggested to be caused either by the formation of iron chlorides, decreasing the adhesion of the oxide scale, or due to sample cooling, motivated by that no indications of spallation nor decohesion of the oxide scale was observed during the ESEM in-situ study. In this study the delamination is concluded to occur during growth, why sample cooling can be excluded as the explanation. Bertrand et al. [32] reported decohesion to occur between the inward and outward growing Fe_3O_4 formed on pure iron after 260 h at 400 °C under chlorine absent conditions. This indicates that the delamination is not necessarily explained by formation of metal chlorides. Pilling and Bedworth [44] proposed that volumetric differences between the substrate and the oxides formed result in compressive stresses in the scale. Clarke et al. [45] also suggested grains of larger lateral size to induce less internal stresses in the oxide scale. The origin of growth stresses has not been investigated systematically in this study. However, the larger oxide grain size observed on the KCl(s) coated sample, compared to the reference, either contradicts the theory of reduced internal stresses or indicates that growth stresses are not the only explanation to the delamination. Further investigations are needed in order to understand why the presence of KCl(s) induces oxide delamination and scale cracking. Larsson et al. [26] showed that the presence of 500 vppm HCl(g) (no KCl(s)) resulted in an oxide scale very similar to the reference sample, but approximately three times thicker, indicating that the very rapid growth and scale delamination observed

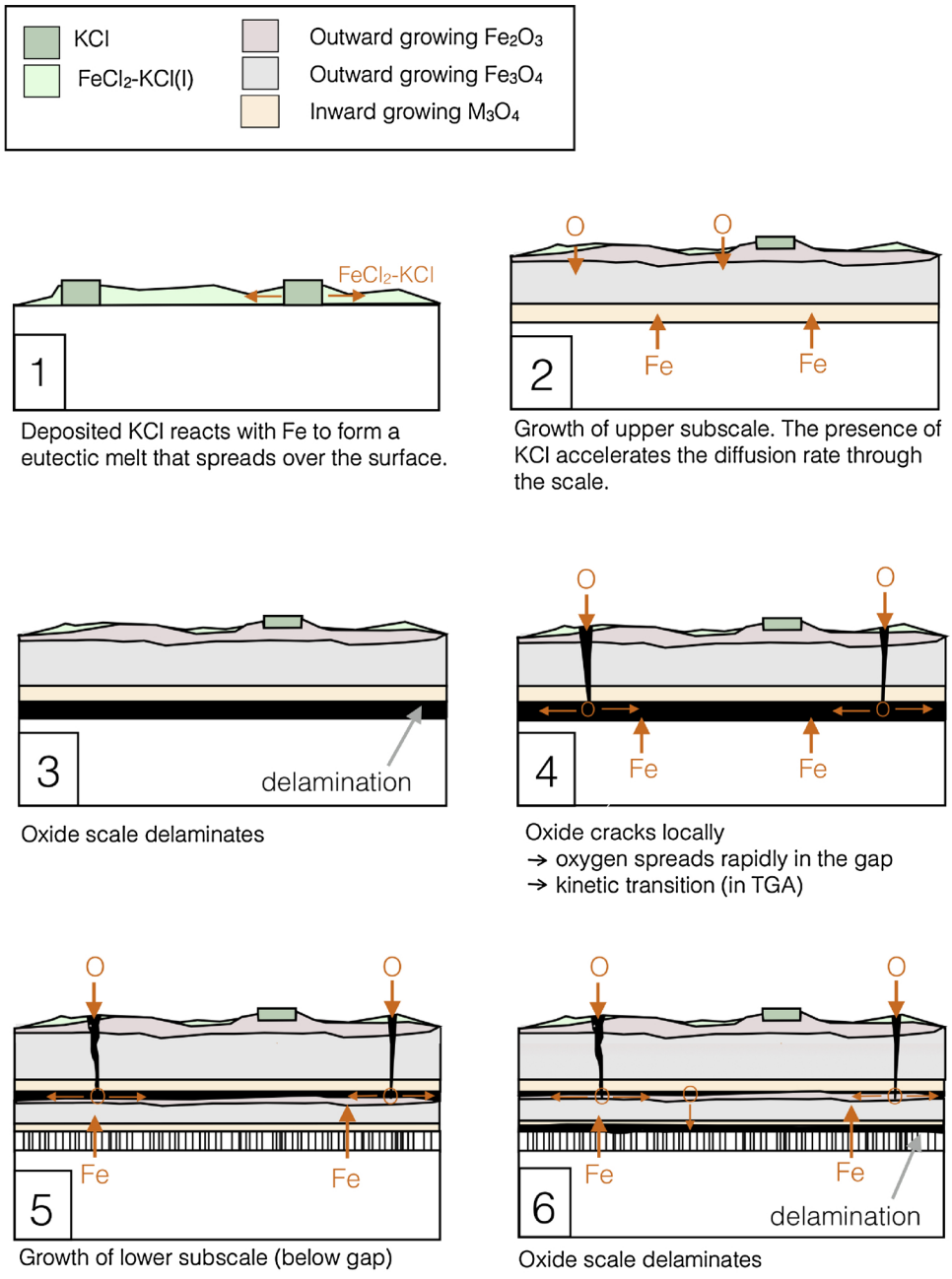

Fig. 8. Schematic representation of the proposed growth process of Fe-2.25-1Mo in exposure conditions with KCl(s) present. The process start with a rapid spread of KCl(s) over the sample surface with subsequent growth of a multi-layered oxide (upper subscale in Fig. 6a). The scale grow relatively thick (3.5–5 µm) during the first few hours and then delaminates from the metal. The oxide scale cracks at local positions and allows for oxygen to enter and rapidly spread through the lateral gap resulting in a global kinetic transition (see Fig. 1). The inflow of oxygen subsequently results in that a new subscale starts to form below the delaminated subscale which is the beginning of the next growth cycle.

in this study is specific for KCl(s) and not general for any chlorine containing compound at 400 °C. The thickness corresponded well with the mass gain data reported by Zahs et al. [3] on pure iron exposed at 400 °C in presence of 500 vppm HCl(g).

4.2.2.1. Microstructural changes. The upper subscale formed on the KCl (s) coated sample is concluded to consists of 30% inward growing and 70% outward growing oxide while the lower subscale consists of 45% inward and 55% outward growing oxide, including the fibre structured oxide, (see Table 2. Thus, the relative amount of inward growing oxide increased in both subscales in presence of KCl(s) compared to the reference exposed sample (compare Tables 2 and 3). This is an indication of that the presence of KCl(s) (chlorine and/or potassium) enhances anion (O^{2-}) diffusion more than cation diffusion.

It may also be noted that the composition of the inward growing oxides varies between the two subscales and that the amount of chromium is not uniform in the inward growing spinel but ranged from 2.5–10 at% (avg. 7 at%) for the upper subscale, 3–5 at% for the dense lower subscale and 16–21 at% Cr for the fibre structured oxide. The higher chromium content can be explained by the iron diffusion outwards by that iron depletion results in higher relative levels of other alloying elements in the inward growing oxide. The higher levels of chromium may influence the diffusion properties of the oxide scale, which is another possible explanation to the increased amount of inward growing scale observed. However, this could not be concluded in this study. Further studies are ongoing in order to investigate how chromium doping of the mixed spinel oxide could influence anionic as well as cationic diffusion.

The accelerated corrosion observed in presence of KCl(s) is in literature often explained by the active oxidation process [2,4,6,8,10,11,28]. The active oxidation process would predict increased amount of outward growing oxide when KCl(s) is present due to

outward diffusion of metal chlorides decomposing into porous oxides. However, the microstructural observations in this study, showing increased amount of inward growing compared to outward growing oxide, may be an indication of that the active oxidation process is not the main, at least not the only, mechanism responsible for the accelerated corrosion observed on Fe-2.25Cr-1Mo in presence of KCl(s) under the investigated exposure conditions. Uusitalo et al. [10] observed a porous and delaminated oxide scale after exposing Fe-2.25Cr-1Mo for 1000 h at 550 °C in 500 vppm HCl(g) + 20% H_2O + 14%CO_2 + 3%O_2 + Ar (bal.). The porous scale was suggested to be caused by active oxidation. By using the same type of interpretation as in this study, the oxide formed in the study by Uusitalo et al. [10] was composed of two delaminated multi-layered scales with approximately 40% inward growing and 60 % outward growing oxides. The comparison between the microstructure of the oxide scale formed without HCl(g) was not the focus of the study by Uusitalo et al. [10]. However, the reference sample in this study, as well as pre-oxidations performed on Fe-2.25Cr-1Mo at 500 °C by Olivas Ogaz et al. [27], suggests that the relative amount of inward growing oxide formed on Fe-2.25Cr-1Mo is lower in absence of chlorine. This observation indicates that another or additional process than the active oxidation could be the reason for the accelerating growth of the oxide scale in presence of chlorine.

The enhanced inward diffusion of oxygen is predicted by the electrochemical mechanism proposed by Folkeson et al. [14,24] who proposed that iron chlorides at the grain boundaries would facilitate ion, especially anion (e.g. O^{2-}), diffusion through the scale. However, no iron chlorides were observed in the grain boundaries in that study. In the present study the STEM/EDX analysis shows traces of chlorine (< 1 at%) in the inward growing oxide in the lower subscale. It is possible that the small amounts of chlorine detected are traces of evaporated metal chlorides that have escaped as a consequence of scale cracking and delamination. However, the performed mass balance and the agreement between calculated and measured thicknesses suggest low levels of evaporated species. The presence of chlorine was qualitatively ensured by comparing the EDX spectra from the KCl(s) coated sample to the reference sample (and the rest of the oxide scale of the KCl(s) coated sample) clearly showing that the chlorine signal is only visible at this position on the KCl(s) coated sample. It should be noted that the amount of chlorine could not be quantified with certainty both due to the porous structure and the overlapping X-ray energies of chlorine and molybdenum present in small amounts in this region. It should also be noted that the chemical detection of STEM/EDX is limited, why minor traces of chlorine could also be present in other regions of the scale. Under the experimental conditions, i.e. the acceleration voltage, the detector limitations and the sample thickness, it would be possible to detect approximately the amount of chlorine corresponding to a decorated oxide grain boundary. Possibly chemical analysis with lower detection limit (e.g. energy loss spectroscopy (EELS) or atom probe tomography (APT)) could be used in order to determine if e.g. any type of metal chloride have formed at the grain boundaries or if chlorine is segregated to other regions.

The scale microstructure observed in presence of KCl(s) in this study is more complex than has previously been reported and consists of a repeated multi-layered scale composed of Fe_2O_3, Fe_3O_4 and $(Fe,Cr,Si,Mo)_3O_4$) with Fe_2O_3 incorporated in several locations in the middle of the scale (low pO_2). The XRD results suggest that both hematite (Fe_2O_3), spinel/magnetite (Fe_3O_4) and maghemite (γ-Fe_2O_3)) are present in the oxide scale. The γ-Fe_2O_3 is, however, not confirmed by TEM or TKD. Possibly the observed γ-Fe_2O_3 phases could be remains from an intermediate phase formed during oxidation at 400 °C since it is well known that γ-Fe_2O_3 may transform into α-Fe_2O_3 between 300–600 °C [46,47]. This could be a possible explanation to the unexpected α-Fe_2O_3 observed to be incorporated in the upper Fe_3O_4 (see Fig. 6c.) However, it is also known that spinel type oxides (M_3O_4) containing Fe^{2+} ions may be oxidised to γ-Fe_2O_3 below 300 °C [46]. It is therefore possible that the γ-Fe_2O_3 has formed after the exposure, why no further conclusions about its influence of the overall growth rate will be drawn in this study.

A porous fibre structured oxide is also observed at the scale/metal interface. The fine, porous structure makes it difficult to determine the phase of this layer by TEM diffraction because of movement from the oxide phase to pores when tilting the sample. However, the TEM diffraction (not shown) indicates that it is crystalline by showing a spot diffraction pattern in this region. The diffraction pattern is not indexed since the XRD data (see Fig. 7 only show signal from Fe_2O_3 (corundum), $(Fe_{1-x},Cr_x)_3O_4$ (spinel) and the alloy (BCC) suggesting that this phase is a spinel type oxide if it is crystalline. The STEM/EDX analysis shows that the oxide is enriched in chromium, molybdenum, and silicon, also suggesting that it is an inward growing spinel [35–37] highly depleted in iron. It is tempting to conclude that the different microstructure is the reason for the delamination observed in this study and that the traces of chlorine could be remains from evaporated metal chlorides explaining the formation of this structure. However, the structure was observed on Fe-2.25Cr-1Mo exposed without chlorine at higher temperature [27] and not observed at the first delamination (in the middle of the scale). The microstructure has only been observed on relatively thick oxide scales (> 3 µm, grown up to 24 h) formed on Fe-2.25Cr-1Mo, suggesting that the structure is correlated to rapid oxide growth. Further studies are ongoing in order to characterise this structure and understand how it could influence the overall growth process of the oxide scale.

5. Conclusions

The presence of KCl(s) accelerates corrosion of the low alloyed steel Fe-2.25Cr-1Mo and changes the oxide microstructure markedly at 400 °C. KCl also reduces cohesion of the oxide scale formed on Fe-2.25Cr-1Mo and makes the oxide scale susceptible to crack formation. Delamination in combination with local cracks results in a global change in oxidation kinetics. Presence of chlorine and/or potassium is proposed to lower the activation energy for diffusion in bulk and/or grain boundaries resulting in an increased diffusion rate. The microstructure and oxidation kinetics indicate that the oxide growth is diffusion controlled with similar diffusion rate before and after delamination/cracking. Presence of KCl increases the relative amount of inward growing scale indicating that the presence of small amounts of chlorine and potassium detected in the scale may facilitate for oxygen diffusion inwards.

Data availability

The raw and processed data required to reproduce these findings cannot be shared at this time due to technical or time limitations.

Acknowledgements

This work was carried out at the Swedish High temperature corrosion Centre (HTC) at Chalmers University of Technology. The authors would also like to acknowledge Patrick Trimby of Oxford instruments for performing the TKD analysis.

References

[1] H.P. Nielsen, F.J. Frandsen, K. Dam-Johansen, L.L. Baxter, The implications of chlorine-associated corrosion on the operation of biomass-fired boilers, Prog. Energy Combust. Sci. 26 (2000) 283–298.
[2] M. Spiegel, A. Zahs, H.J. Grabke, Fundamental aspects of chlorine induced corrosion in power plants, Mater. High Temp. 20 (2) (2003) 153–159.
[3] A. Zahs, M. Spiegel, H.J. Grabke, Chloridation and oxidation of iron, chromium, nickel and their alloys in chloridizing and oxidizing atmospheres at 400–700 °C, Corros. Sci. 42 (6) (2000) 1093–1122.
[4] Y.S. Li, Y. Niu, W.T. Wu, Accelerated corrosion of pure Fe, Ni, Cr and several Fe-based alloys induced by $ZnCl_2$-KCl at 450 °C in oxidizing environment, Mater. Sci.

Eng. A345 (2003) 64–71.
[5] F. Wang, Y. Shu, Influence of Cr content on the corrosion of Fe-Cr alloys: the synergistic effect of NaCl and water vapor, Oxid. Met. 59 (3–4) (2003) 201–214.
[6] S.C. Cha, M. Spiegel, Local reactions of KCl particles with iron, nickel and chromium surfaces, Mater. Corros. 57 (2) (2006) 159–164.
[7] H.T. Ma, C.H. Zhou, L. Wang, High temperature corrosion of pure Fe, Cr and Fe-Cr binary alloys in O_2 containing trace KCl vapour at 750 °C, Corros. Sci. 51 (8) (2009) 1861–1867.
[8] H.J. Grabke, E. Reese, M. Spiegel, The effects of chlorides, hydrogen-chloride, and sulfur-dioxide in the oxidation of steels below deposits, Corros. Sci. 37 (7) (1995) 1023–1043.
[9] A. Zahs, M. Spiegel, H.J. Grabke, The influence of alloying elements on the chlorine-induced high temperature corrosion of Fe-Cr alloys in oxidizing atmospheres, Mater. Corros. 50 (10) (1999) 561–578.
[10] M.A. Uusitalo, P.M.J. Vuoristo, T.A. Mantyla, High temperature corrosion of coatings and boiler steels in oxidizing chlorine-containing atmosphere, Mater. Sci. Eng. A – Struct. Mater. Prop. Microstruct. Process. 346 (1–2) (2003) 168–177.
[11] M.A. Uusitalo, P.M.J. Vuoristo, T.A. Mantyla, High temperature corrosion of coatings and boiler steels below chlorine-containing salt deposits, Corros. Sci. 46 (6) (2004) 1311–1331.
[12] J. Pettersson, H. Asteman, J.E. Svensson, L.G. Johansson, KCl induced corrosion of a 304-type austenitic stainless steel at 600 °C: the role of potassium, Oxid. Met. 64 (1–2) (2005) 23–41.
[13] S. Sroda, S. Tuurna, Laboratory scale tests on corrosion behavior of boiler materials in simulated combustion atmospheres (EU Project – OPTICORR), Mater. Corros. 57 (3) (2006) 244–251.
[14] N. Folkeson, L.G. Johansson, J.E. Svensson, Initial stages of the HCl-induced high-temperature corrosion of alloy 310, J. Electrochem. Soc. 154 (9) (2007) C515–C521.
[15] J. Pettersson, J.E. Svensson, L.G. Johansson, Alkali induced corrosion of 304-type austenitic stainless steel at 600 °C: comparison between KCl, K_2CO_3 and K_2SO_4, Mater. Sci. Forum 595–598 (2008) 367–375.
[16] C. Pettersson, L.G. Johansson, J.E. Svensson, The influence of small amounts of KCl (s) on the initial stages of the corrosion of alloy Sanicro 28 at 600 °C, Oxid. Met. 70 (5–6) (2008) 241–256.
[17] T. Jonsson, B. Pujilaksono, S. Hallstr“om, J. Ågren, J.E. Svensson, L.-G. Johansson, M. Halvarsson, An ESEM in-situ investigation of the influence of H_2O on iron oxidation at 500 °C, Corros. Sci. 51 (9) (2009) 1914–1924.
[18] C. Proff, T. Jonsson, C. Pettersson, J.E. Svensson, L.G. Johansson, M. Halvarsson, Microstructural investigation of the KCl-induced corrosion of the austenitic alloy Sanicro 28 (35Fe27Cr31Ni) at 600 °C, Mater. High Temp. 26 (2) (2009) 113–125.
[19] S. Karlsson, J. Liske, L.-G. Johansson, J.-E. Svensson, Alkali induced high temperature corrosion of stainless steel: the influence of NaCl, KCl and $CaCl_2$, Oxid. Met. 78 (2012) 83–172.
[20] J. Sui, J. Lehmusto, M. Bergelin, H. Mikko, The effects of KCl, NaCl and K_2CO_3 on the high-temperature oxidation onset of Sanicro 28 steel, Oxid. Met. 85 (2016) 565–598.
[21] D. Bramhoff, H.J. Grabke, E. Reese, H.P. Schmidt, Einfluß von HCl und Cl2auf die Hochtemperaturkorrosion des 2 1/4 Cr 1 Mo-Stahls in Atmosph”aren mit hohen Sauerstoffdr“ucken, Mater. Corros. 41 (6) (1990) 303–307.
[22] E. Reese, H.J. Grabke, Einflun von Chloriden auf die Oxidat ion, Werkstoffe und Korrosion 43 (1992) 547–557.
[23] S. Środa, S. Tuurna, K. Penttil”a, L. Heikinheimo, High temperature oxidation behaviour of boiler steels under simulated combustion gases, Mater. Sci. Forum 461–464 (2004) 981–988.
[24] N. Folkeson, T. Jonsson, M. Halvarsson, L.G. Johansson, J.E. Svensson, The influence of small amounts of KCl(s) on the high temperature corrosion of a Fe-2.25Cr-1Mo steel at 400 and 500 °C, Mater. Corros. 62 (7) (2011) 606–615.
[25] T. Jonsson, N. Folkeson, J.-E. Svensson, L.-G. Johansson, M. Halvarsson, An ESEM in situ investigation of initial stages of the KCl induced high temperature corrosion of a Fe-2.25Cr-1Mo steel at 400 °C, Corros. Sci. 53 (2011) 2233–2246.
[26] E. Larsson, The Corrosive Effect of Chlorine Containing Species on Waterwalls and Superheater Materials in Waste and Biomass-Fired Power Plants (Ph.D. dissertation), Chalmers University of technology, 2016.
[27] A.M. Olivas Ogaz, J. Eklund, A. Persdotter, M. Sattari, J. Liske, J.-E. Svensson, T. Jonsson, The influence of oxide-scale microstructure on KCl(s)-induced corrosion of low-alloyed steel at 400 °C, Oxid. Met. 91 (3–4) (2019) 291–310.
[28] M.J. McNallan, W.W. Liang, S.H. Kim, C.T. Kang, Acceleration of the High Temperature Oxidation of Metals by Chlorine, High Temperature Corrosion, NACE, 1983, pp. 316–321.
[29] P. Kofstad, High Temperature corrosion, Elsevier Applied Science, London/New York, 1988.
[30] V. Cantatore, M.A. Olivas Ogaz, J. Liske, T. Jonsson, J.-E. Svensson, L.-G. Johansson, I. Panas, Oxidation driven permeation of iron oxide scales by chloride from experiment guided 1st principles modelling, J. Phys. Chem. C (2019).
[31] H. Hooshyar, J. Liske, L.G. Johansson, M. Seemann, T. Jonsson, Initial corrosion attack of 304L and T22 in 2 MW biomass gasifier: a microstructural investigation, Mater. High Temp. 32 (1–2) (2015) 197–204.
[32] N. Bertrand, C. Desgranges, D. Gauvain, D. Monceau, D. Poquillon, Low temperature oxidation of pure iron: growth kinetics and scale morphologies, Mater. Sci. Forum 461–464 (2004) 591–598.
[33] T. Jonsson, J. Froitzheim, J. Pettersson, J.E. Svensson, L.G. Johansson, M. Halvarsson, The influence of KCl on the corrosion of an Austenitic stainless steel (304L) in oxidizing humid conditions at 600 °C: a microstructural study, Oxid. Met. 72 (3–4) (2009) 213–239.
[34] B. Pujilaksono, T. Jonsson, M. Halvarsson, J.-e. Svensson, L.-g. Johansson, Oxidation of iron at 400–600 °C in dry and wet O_2, Corros. Sci. 52 (5) (2010) 1560–1569.
[35] B. Pujilaksono, T. Jonsson, H. Heidari, M. Halvarsson, J.E. Svensson, L.G. Johansson, Oxidation of binary FeCr alloys (Fe-2.25Cr, Fe-10Cr, Fe-18Cr and Fe-25Cr) in O_2 and in O_2 + H_2O environment at 600 °C, Oxid. Met. 75 (3–4) (2011) 183–207.
[36] J. T“opfer, S. Aggarwal, R. Dieckmann, Point defects and cation tracer diffusion in $(Cr_xFe_{1-x})_{3-\delta}O_4$ spinels, Solid State Ionics 81 (2738) (1995) 251–266.
[37] J.A.V. Orman, K.L. Crispin, Diffusion in oxides, Rev. Mineral. Geochem. 72 (2010) 757–825.
[38] J.-O. Andersson, T. Helander, L. H”oglund, P. Shi, B. Sundman, Thermo-Calc & DICTRA, computational tools for materials science, Calphad 26 (2) (2002) 273–312.
[39] Y. Alipour, P. Henderson, Corrosion of furnace wall materials in waste-wood fired power plant, Corros. Eng. Sci. Technol. 50 (5) (2015) 355–363.
[40] A. Talus, Y. Alipour, R. Norling, P. Henderson, Effect of sewage sludge addition on initial corrosion of 16Mo3 and 310S when exposed in a used wood fired boiler, Mater. Corros. 67 (7) (2016) 683–692.
[41] M.J.G. da Silva, Influence of Oxide Microstructure on Corrosion Behavior of Zirconium-Based Model Alloys (Ph.D. dissertation), The Pennsylvania State University, 2007.
[42] C. Juricic, H. Pinto, D. Cardinali, M. Klaus, C. Genzel, A.R. Pyzalla, Effect of substrate grain size on the growth, texture and internal stresses of iron oxide scales forming at 450 °C, Oxid. Met. 73 (2010) 15–41.
[43] K. Jiang, X. Yang, Z. Wu, Mössbauer study of the effect of potassium on iron oxide catalysts, Hyperfine Interact. 77 (1993) 67–70.
[44] N. Pilling, R. Bedworth, The oxidation of metals at high temperatures, J. Inst. Met. 29 (1923) 529–582.
[45] D.R. Clarke, The lateral growth strain accompanying the formation of a thermally grown oxide, Acta Mater. 51 (2003) 1393–1407.
[46] B. Gillot, R.M. Benloucif, F. Jemmali, Some electrical properties of the defective γ phases of spinel structure during their transformation to the rhombohedral α phases, J. Mater. Sci. 19 (11) (1984) 3806–3813.
[47] E. Herrero, M. Cabanas, M. Vallet-Regi, J.L. Martinez, J.M. Gonzalez-Calbet, Influence of synthesis conditions on the γ-Fe_20_3 properties, Solid State Ionics 101 (101–103) (1997) 213–219.
[48] K. Yagi, Creep properties of heat resistant steels and superalloys ċ 2.25Cr-1Mo steel, in: H.W.K. Yagi, G. Merckling, T.-U. Kern, H. Irie (Eds.), Creep Properties of Heat Resistant Steels and Superalloys, Group VIII Advanced Materials and Technologies, vol. 2B, SpringerMaterials, 2004, p. 67.